ELSEVIER

Thin Solid Films 349 (1999) 135–146

thin solid films

Fabrication and characterisation of thin low-temperature MBE-compatible silicon oxides of different stoichiometry

A. Strass[a,*], P. Bieringer[a], W. Hansch[b], V. Fuenzalida[c], A. Alvarez[c], J. Luna[c], I. Martil[d], F.L. Martinez[d], I. Eisele[a]

[a]Universität der Bundeswehr München, Fakultät für Elektrotechnik, Institut für Physik, Werner-Heisenberg-Weg 39, 85579 Neubiberg, Germany
[b]Hiroshima University, Research Center for Nanodevices and Systems, 1-4-2 Kagamiyama, Higashi-Hiroshima 739, Japan
[c]Universidad de Chile, Facultad de Ciencias Fisicas y Matematicas, Departamento de Fisica, Avenida Blanco Encalada 2008, Casilla 487-3, Santiago, Chile
[d]Universidad Complutense, Departamento de Fisica Aplicada III, Facultad de Ciencias Fisicas, Madrid 28040, Spain

Received 16 July 1998; received in revised form 11 January 1999; accepted 8 February 1999

Abstract

We developed and tested three MBE-compatible processes for the deposition of high-quality low-temperature silicon oxides and oxynitrides in the ultra high vacuum at substrate temperatures between room temperature and 500°C: gas enhanced evaporation (GEE), plasma enhanced evaporation (PEE) and plasma enhanced oxidation (PEO). The deposited layers were thoroughly investigated and compared with respect to their electrical, optical and stoichiometrical properties by means of ellipsometry, mechanical profilometry, Auger electron spectroscopy (AES), X-ray photoelectron spectroscopy (XPS), Rutherford backscattering (RBS), Fourier transform infrared (FTIR) spectroscopy, and by electrical measurements (*I–V*, *C–V*) on MOS structures. A model of the growth mechanism for each of the processes is suggested. © 1999 Elsevier Science Ireland Ltd. All rights reserved.

Keywords: Atomic and molecular studies; Deposition process; Plasma processing and deposition; Silicon oxide

1. Introduction

SiO_2 thin films are the most important dielectrics and passivation layers in large and ultra-large scale integration of micro- and nanoelectronic devices like non-volatile memories and LOGICs [1–3] or Josephson cache memories [4]. Low-temperature SiO_x are widely employed for their unique electrical, optical and mechanical properties. Substoichiometric oxides in intermetal dielectric stacks can improve the electronic properties of multilevel interconnection devices because they can better water molecules. The high number of dangling bonds in Si rich SiO_x enhances the chemical reactivity for oxides. Thus, water molecules can be subtracted from the surrounding layers [2]. Optoelectronic applications of SiO_x films include facet coatings of semiconductor lasers [5], resonant cavity photodetectors [6] and waveguides [7].

New photonic devices as well as electronic devices with a long-term reliability awakened a high interest in silicon nitrides and silicon oxynitrides for encapsulation and passivation in packaging of integrated circuits, or as an insulating layer in metal-nitride-oxide-silicon (MNOS) devices [8]. Further applications include the use as gate dielectric in thin film transistors (TFT) [9], and as an antireflective protection layer in solar cells [10]. Nitrides are also attractive candidates for realizing smaller dimensions in ICs because of their high dielectric constant (7.0) compared to SiO_2 (3.9) and because of their role as a diffusion layer against moisture and impurity ions. According to the SIA technology roadmap for semiconductors [11] low-leakage dielectrics with high permittivity will be required for DRAM storage node capacitors and on-chip filtering/decoupling.

For many purposes, high quality Si-based dielectrics are produced by high-temperature oxidation or nitridation between 700 and 1000°C. Although, such insulators in general meet all requirements for modern devices, serious problems arise where thermal budget of the process is concerned. For example, MBE-grown nanostructure devices need sharp doping profiles or heterostructures on a nanometer scale for good electronic properties [12]. Process temperatures below 700°C are desirable to avoid dopant redistribution. To prevent interdiffusion of metallic layers like aluminum the process temperature must not exceed

* Corresponding author. Tel.: + 49-8121-71227; fax: + 49-8121-973763.
E-mail address: achim.strass@infineon.com (A. Strass)

0040-6090/99/$ - see front matter © 1999 Elsevier Science Ireland Ltd. All rights reserved.
PII: S0040-6090(99)00166-2

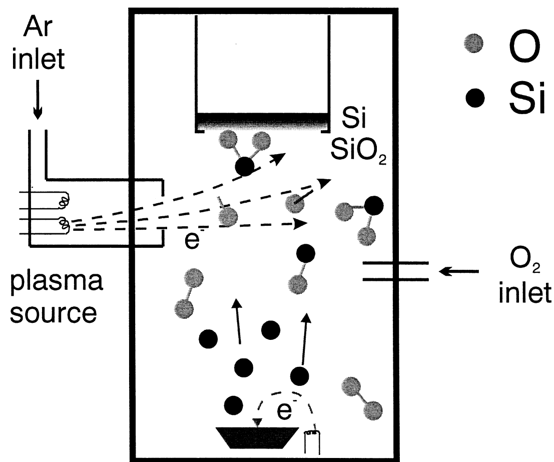

Fig. 1. Process chamber developed for plasma enhanced evaporation and similar processes.

500°C. Hence, very low substrate temperatures are desirable for the fabrication of such devices.

So far, SiO_2 and substoichiometric silicon oxides have been fabricated by PECVD with silane and an oxidizing gas at temperatures below 450°C [13]. However, silane is a dangerous precursor and special care must be taken with the exhaust. One serious disadvantage is the high incorporation of hydrogen into the films coming from the SiH_4 molecule. This leads to unwanted compounds like Si–H or Si–OH which serve as charge traps. This has negative impacts on the dielectric characteristics. Another approach has been the evaporation of solid silicon monoxide (SiO) targets in oxygen atmosphere [5]. Using this target material, however, does not allow the fabrication of SiO_x with $x < 1$. Furthermore, it can be difficult to control the evaporation of SiO by electron beam heating because of its thermal decomposition and particle splitting.

Hence, novel low-temperature oxidation processes have been investigated recently. PEO (plasma enhanced oxidation) delivers oxides by burning a low-energy electron arc in oxygen atmosphere with the Si substrate merged into the plasma. It is eligible for the growth of very thin dielectric layers between 5 and 30 nm. For PEE (plasma enhanced evaporation), Si is evaporated in addition to the plasma. We mainly use it for the fabrication of Si-based nitrides or oxynitrides with a thickness of 20–300 nm. GEE (gas enhanced evaporation) works like PEE only with the plasma switched off because, unlike nitrogen, oxygen naturally reacts with silicon. These techniques offer many advantages over conventional oxide fabrication methods such as accurate determination of the flux, low background contamination, in-situ process monitoring tools, safe operation and a wide process window. All processes can be performed at room temperature and are UHV- and MBE-compatible as they can be easily performed directly after MBE growth in the same chamber without interrupting the UHV conditions.

It is the objective of this paper to compare the electronic, optoelectronic and stoichiometric properties of the oxide films fabricated by the above mentioned low-temperature processes. Many characterisation methods were used to collect as much information on the films as possible because single techniques are all limited. Also, the experimental results are the basis for a discussion of the dynamics of film growth. Fields of applications are suggested.

2. Experimental setup and film growth

The UHV chamber is tested for multiple use such as MBE, oxide growth and hydrogen plasma cleaning of the substrates prior to any further process. The process chamber [14], is part of the Modular UHV multichamber system (MUM 545) from Balzers AG, Liechtenstein [15]. The base pressure in the chamber is typically 5×10^{-9} mbar. All oxides were deposited on high-ohmic p-type (100) oriented silicon substrates. Generally, after a standard RCA cleaning the wafers were immediately introduced into the load-lock of the modular UHV multichamber system. Our standard hydrogen plasma cleaning was applied to remove the native oxide and organic contamination from the substrate surface at room temperature. The principle of the processes is illustrated in Fig. 1 and is described in the following paragraphs.

2.1. Gas enhanced evaporation (GEE)

For subsequent deposition of SiO_x layers silicon was evaporated from a crucible under O_2 gas atmosphere. The deposited Si atoms naturally react with the O_2 molecules at the surface. The deposition rate of Si under UHV conditions was determined by a quadrupole mass spectrometer (QMG) before oxygen was introduced. The gas pressure in the chamber was kept constant by mass flow controllers. Films were grown with oxygen flows ranging from 0.8 sccm (1.5×10^{-3} Pa) to 73 sccm (0.1 Pa) at a substrate temperature of 360°C for most of the samples. The evaporation rate of Si in the UHV was kept constant at 0.3 Å/s. The growth rate of SiO_x depends on the reduced mean free path of the evaporated molecular beam at high gas pressures and on the growth kinetics at the substrate surface. The mean free path falls below 45 cm, which is the distance between the substrate and the Si target, at an oxygen pressure of greater than approximately 4×10^{-2} Pa. One sample was grown in pure N_2 gas atmosphere at a substrate temperature of 360°C.

2.2. Plasma enhanced evaporation (PEE)

Gases like N_2 which do not naturally react with silicon are cracked by a low-energy plasma to form Si_3N_4 or together with O_2 oxynitride insulators [14], but for a better point of view the principle is summarized briefly. A low-energy electron arc of high volume is created by a DC discharge from the negative-biased filament to the grounded chamber walls (anode). The substrate, merged into the plasma, is also

grounded. The average kinetic energy of the electrons is estimated to be 5–10 eV which is enough to dissociate but not ionize the process gas [16]. Thereby, substrate damage is avoided. In addition to O_2, a minimum amount of 20 sccm Ar (6×10^{-2} Pa) is needed as a working gas to create the plasma. Thus, the total process pressure is typically higher than 8×10^{-2} Pa. This low Ar flow was used for all PEE processes to keep the mean free path in the gas as large as possible. Numerous SiO_x and SiO_xN_y films were grown with different Si evaporation rates at room temperature and at 360°C. The oxygen gas flow was varied between 1.5 sccm (2.3×10^{-3} Pa) and 15 sccm (2.6×10^{-2} Pa). Oxynitrides were grown with an O_2/N_2 flow of 0/8, 2/6 and 4/4 sccm at 360°C.

2.3. Plasma enhanced oxidation (PEO)

A third method of growing SiO_2 is by plasma enhanced oxidation (PEO). It works like PEE only with the evaporator switched off. The Ar flow was maintained at 80 sccm (1.2×10^{-1} Pa) for most of the samples because under this condition the plasma was found to be very stable and of good geometry. The oxygen flow was fixed at 10 sccm. The process pressure was typically 0.5 Pa. Plasma oxynitrides were grown with an O_2/N_2 flow of 0/10 sccm (room temperature and 360°C) and 5/5 sccm (360°C).

3. Film characterisation methods

The thickness and the refractive index of the as-deposited oxide layers were determined at fixed wavelength (633 nm) and fixed incident angle (70°) with a PLASMOS SD 2300 ellipsometer. The measurements were carried out systematically in N-float and N-fix modus at several points for each sample. The validity of the thickness measurements was confirmed by comparison with the results obtained from a mechanical profilometer (Sloan Dektak II).

For electrical characterization, Al pads were evaporated on the films through a mechanical shadow mask to form metal-insulator-semiconductor (MIS) diodes with an area of 7.8×10^{-3} cm^2. The electrical back side contact to the metal chuck was ensured by conducting silver. We avoided sputtering the back side because in our experiments it sometimes caused electrical damage to very thin dielectric films. Capacitance-voltage (*C–V*) and conductance-voltage (*G–V*) measurements were obtained from a HP4275 multi frequency LRZ meter. A Keithley-230 programmable voltage source as well as a Keithley-617 programmable electrometer were used for dynamic ramp current-voltage (*I–V*) measurements. The current was measured 3 s after the applied voltage was increased in steps of 0.3 V.

Electrical and optical properties of dielectrics are very sensitive to stoichiometry and impurities. Thus, we characterized the stoichiometry and impurity level by electron spectroscopy (AES and XPS), as well as by RBS and FTIR.

Prior to surface electron spectroscopy the samples have to be sputter-cleaned for two reasons. The surface is usually covered with adsorbed carbon, hydrocarbons or carbon oxides leading to a weaker signal of the SiO_x compound and to errors in the determination of the atomic concentration of the elements. Furthermore, when exposed to air, native SiO_2 is formed on SiO_x surfaces with $x < 2$. To reduce damage, the samples were first sputtered by ions of higher kinetic energy and subsequently by a beam of lower energy.

Auger electron spectroscopy (AES) enables the determination of relative atomic concentrations and - to a certain extent - chemical analysis of a film. AES measurements were performed on a Perkin–Elmer ESCA/Auger system, PHI model ESCA 550, with a double pass cylindrical mirror analyzer. The base pressure in the analysis chamber was typically 1.0×10^{-7} Pa. The samples were all sputter-cleaned prior to analysis by an Ar^+ ion beam of 3 kV for 60 s and 1 kV for another 60 s from a differentially pumped Perkin–Elmer, PHI model 04-303 ion gun. Next to rough surveys, high resolution spectra were recorded with a kinetic energy of 3 kV of the incident electron beam for Si LVV and O KLL and of 5 kV for Si KLL. These energies were used to obtain strong signals for Si LVV and Si KLL, respectively. The current through the sample was fixed to 300 nA in each case. It should be noted that a quantitative analysis of the atomic concentration of Si and O is hardly possible in substoichiometric SiO_x. The peak for Si LVV splits for substoichiometric SiO_x with maxima at 76 eV (for SiO_2) and 92 eV (for elemental Si) in the differentiated surface spectrum [17].

X-ray photoelectron spectroscopy, also known as electron spectroscopy for chemical analysis (ESCA) was used to determine the chemical state of the oxides as well as the atomic concentrations of the elements. For XPS measurements a Perkin–Elmer, PHI model 1257, ESCA spectrometer with a concentric hemispherical electron analyzer was used with a pass energy of 20 eV. The pressure in the analysis chamber was typically 2×10^{-8} Pa. Photoelectrons were excited by Mg K_α X-rays with $h\nu = 1253.6$ eV. The binding energy scale was calibrated with the C 1s photoelectron line at 284.6 eV to correct the charging effect. All experiments were performed at a takeoff angle of 54°, (the so called magic XPS angle) with respect to the surface plane. For Ar^+ sputtering a Perkin–Elmer, PHI model 04-303 ion gun was applied. The samples were first bombarded by 2 keV ions (5 mC charge in total) and subsequently by 1 keV ions (2 mC) for a mild treatment. The sputtered area was about 0.5 cm^2.

Rutherford Backscattering (RBS) measurements were done to find out the atomic composition of the films. Analyses were done on a High Voltage Engineering Europe B.V. accelerator and end station. The incident beam consisted of 1 MeV 4-He^+ ions and was directed perpendicular to the sample surface. RBS data were collected at a backscatter angle of 75°. Since the information is obtained

Table 1
Typical values for film thickness, growth rate and refractive index of SiO_2 fabricated by three different growth methods. The values given for the refractive index of PEE-grown SiO_2 is only valid for films thicker than 150 Å

	Gas enhanced evaporation (GEE)	Plasma enhanced evaporation (PEE)	Plasma enhanced oxidation (PEO)
Layer thickness (Å)	400–600	200–2000	40–300
Lateral uniformity (%)	< 3	2–6	2–6
Growth rate (Å/s)	0.25–0.80	0.2–3	0.03–0.2
Refractive index	1.42–1.48	1.45–1.49	1.44–1.47
Lateral uniformity (%)	< 1	< 2	0.5–2

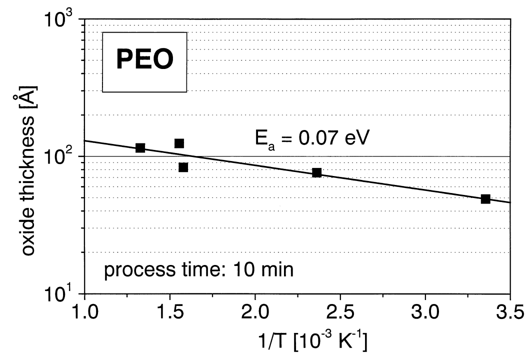

Fig. 3. Arrhenius plot of PEO oxide thickness as a function of inverse temperature.

from nuclei scattering, no chemical data are available by this method.

Fourier transformed transmission infrared (FTIR) absorption spectra were taken from SiO_x samples to study the bonding configuration in the bulk of the films. The location of the absorption band identifies the chemical bond, the concentration of the bond determines the intensity of the peak. A Nicolet 5PC FTIR spectrometer operating in the mid-infrared region (400–4000 cm^{-1}) was used to obtain the data. The recorded data are corrected by a fitted baseline (to account for interference effects in the film) and subtracting the spectra of a bare silicon substrate to eliminate the silicon peaks.

Three samples were used as a reference for the performed measurements: elemental Si, wet thermal SiO_2, and CVD-Si_3N_4.

4. Experimental results

In this section the experimental results are presented and – if possible – compared for the three low-temperature oxide fabrication processes. The measured film properties and the experiments on dynamics of film growth are the basis for the discussion in the following section.

Table 1 gives an overview over typical values for refractive index, film thickness and growth rate for all three processes. The very low growth rates for PEO clearly show that pure plasma oxide growth is not a competitive process to PEE where film growth is accelerated by evaporation. Because of the similarity of both growth methods, the typical lateral uniformity in thickness for the GEE-samples corresponds to that of pure Si MBE deposition of Si in the UHV. The PEE and PEO samples show a higher thickness at locations closer to the plasma source. This could be improved by a sweeping arc and by substrate rotation or by a different chamber geometry. The lateral uniformity in the refractive index is below 2% for all samples.

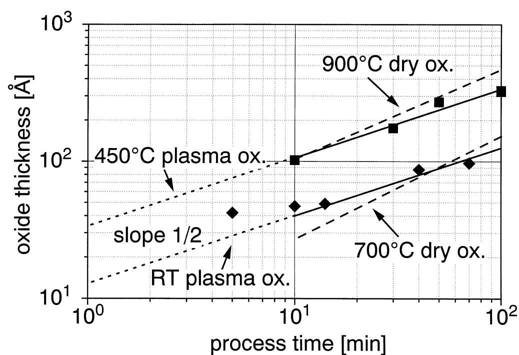

Fig. 2. Double-logarithmic plot of the PEO oxide thickness versus duration to O_2 plasma exposure. The dashed lines for dry oxidation are shown for comparison [19].

Fig. 2 shows a double logarithmic plot of the PEO oxide thickness versus the duration of exposure to the oxygen plasma. Above 10 min the thickness of the grown SiO_2 layers is directly proportional to the square root of the process time. This time dependence is conferred from the slope (1/2) of the plot indicating that the oxidation kinetics is limited by the diffusion of oxidizing species through the growing film rather than by the flux of species to the surface. Hence, for a thickness of more than 50 Å the growth is obviously transport rate limited and thus comparable to thermal oxidation where the relatively large oxygen molecules diffuse through the oxide layer, followed by the reaction at the Si/SiO_2 interface, first described by Deal and Grove [18]. Films grown in a pure N_2 plasma are only half as thick as those grown in a pure O_2 plasma under the same or similar conditions.

Compared to thermal oxidation, film growth by PEO proceeds much more rapidly leading to the conclusion that the plasma supplies particles that diffuse easier as compared to O_2 molecules. With our conditions, plasma oxidation rates at room temperature and 450°C are nearly the same as compared with those found in standard literature for dry thermal oxidation at 700 and 900°C, respectively [19]. The slope for thermal oxides is actually a bit higher than 1/2 because the Deal–Grove model is valid for thicknesses above 300 Å. Furthermore, the SiO_2 growth rates show Arrhenius dependence versus substrate temperature with a positive activation energy of 0.07 eV (Fig. 3). This value is nearly three times smaller than the value of 0.19 eV found

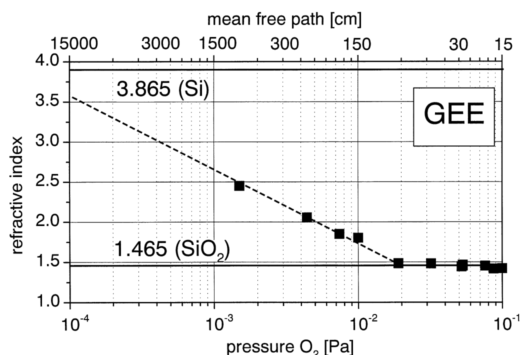

Fig. 4. Refractive index of GEE-grown SiO_x as a function of O_2 pressure during Si evaporation.

by Hu et al, in a similar experiment [20]. The activation energy is significantly smaller than for dry thermal oxidation where it amounts to 2.22 eV [18].

The refractive index of the GEE-grown samples, measured by ellipsometry, can be easily set by varying the O_2 flow into the chamber as shown in Fig. 4. Above 2×10^{-2} Pa the mean free path of the Si atoms is lower than the distance between the crucible with the Si target and the substrate which is 45 cm. The refractive index indicates that stoichiometric SiO_2 is formed under these conditions. Below 2×10^{-2} Pa the refractive index of the deposited layer exponentially grows with decreasing O_2 pressure in the chamber. By extrapolation, the refractive index of crystalline Si (3.8) should be reached at an approximate oxygen pressure of 5×10^{-5} Pa. It should be mentioned that the accuracy of ellipsometric measurements decreases for very Si rich oxides because of lower transparency at the wavelength of 633 nm.

4.1. Auger electron spectroscopy (AES)

All oxide films as loaded into the AES analysis chamber only show surface contamination by C. After the sputter cleaning the concentration of C fell below the detection limit of 1%. Fig. 5 displays changes in Si LVV and Si KLL as a function of the refractive index n for a selection of GEE oxides. These results are compared with measurements obtained from thermal SiO_2 and pure Si. The Si LVV peak at 92 eV increases at the expense of the peak at 76 eV for increasing Si:O ratio x. The Si KLL peak moves from 1622.5 eV for $x = 2$ to 1612.5 eV for $x = 0$. The position of the O KLL is located around 505 eV for all samples (not shown here). Slight deviations to the literature values [17] are due to charging effects. The AES peak locations show the presence of Si, SiO_2 and SiO_x phases in substoichiometric silicon oxide films (samples GEE6, GEE5, GEE4 from Table 2). The Si LVV peak of the near stoichiometric GEE specimen (GEE3, GEE1, GEE2) is not as sharp as that of the thermal SiO_2. This indicates that slight amounts of silicon-rich clusters are incorporated into the films by the evaporation process or that the layers are not as dense as

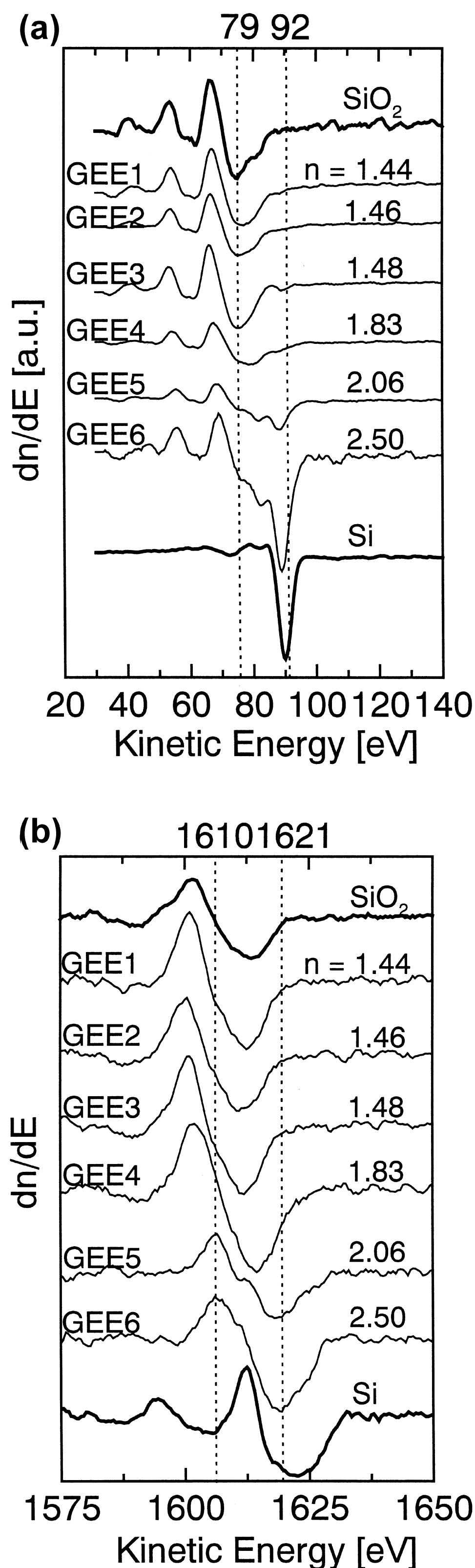

Fig. 5. Changes of the (a) Si KLL and (b) Si LVV Auger spectra of GEE oxides as a function of refractive index. The curves of thermal SiO_2 and of elemental Si are shown for comparison. The dashed lines give the literature values of the bottom peak of Si LVV (76 eV for SiO_2, 92 eV for Si) and Si KLL (approximately 1610 eV for SiO_2, 1621 eV for Si) [17].

Table 2
Comparison of two GEE- and PEE-deposited films with respect to refractive index and stoichiometry. The thicknesses values in parentheses are measured by mechanical profilometry. Ellipsometer measurements were not possible due to high absorption at 632 nm wavelength

WAFER	O_2 partial pressure (mbar)	Gas flow (sccm) O_2	Gas flow (sccm) N_2	Refractive index	Ratio Si:O (%) (RBS)	Ratio Si:O:N (%) (XPS)	Ratio x O:Si x (XPS)	Thickness (ellipsom) (Å)
GEE1	5.4×10^{-4}	30	–	1.44	31:69	33:67	2	680
GEE2	5.2×10^{-4}	30	–	1.47	33:67	33:67	2	454
GEE3	1.9×10^{-4}	10	–	1.48	–	33:67	2	567
GEE4	1.0×10^{-4}	7	–	1.83	–	36:64	1.75	547
GEE5	4.4×10^{-5}	2.3	–	2.06	40:60	42:58	1.38	520
GEE6	1.5×10^{-5}	0.8	–	2.50	48:52	52:48	0.92	460
PEE1	1.4×10^{-4}	10	–	1.466	–	33:67	2	1704
PEE2	1.4×10^{-4}	10	–	1.474	–	33:67	2	1489
PEE3	2.4×10^{-5}	1.5	–	–	–	71:29	0.41	1050
PEE4	2.1×10^{-5}	1.5	–	–	–	76:24	0.32	1043
PEE5	–	0	8	1.91	–	35:16:49	–	371
PEE6	2.7×10^{-5}	2	6	1.51	–	25:73:3	–	334
PEE7	7.0×10^{-5}	4	4	1.57	–	36:64:0	–	282

thermal SiO_2, which may cause changes in the angle of the SiO_2 molecule. When the Si and O atomic concentrations are nearly equal (sample GEE6), the film consists of a mixture of all SiO_x phases ($x = 0$, 1, 1.5, 2) as indicated by the broad peak. This will be confirmed by XPS data as shown below. No incorporated nitrogen was found neither by AES nor by XPS in the deposited Si layer of the GEE sample grown in N_2 gas atmosphere.

AES spectra were also taken for PEE grown samples with different N_2:O_2 gas mixtures in the plasma in order to grow oxynitrides. No N was found for PEE7, where the N_2:O_2 flow ratio was lowest (compared to PEE5 and PEE6), neither by AES nor by XPS. The atomic concentration of N for PEE6 was determined to 7%. The depth profile as well as a surface spectrum of sample PEE5 after 3 min sputtering, which was deposited by PEE in the nitrogen plasma, is shown in Fig. 6. After correction for relative sensitivities, the film is composed of 35% Si, 49% N and 16% O. The relatively high incorporation of O is attributed to the desorption of residual oxygen from the process chamber by plasma radicals. The high Si content indicates that, even though activated by the plasma, nitrogen is very reluctant to react with the deposited Si species. A fairly vertical uniform distribution is followed by a rather abrupt transition region. In this region, the Si content increases concurrently with the decreasing nitrogen content while the O profile faces a slight maximum at the interface. This is also due to residual oxygen which reacts much easier with the dangling bonds of the Si surface than nitrogen at the beginning of film growth. Even a CVD-Si_3N_4 sample contains 7% oxygen. Fig. 7 summarizes the spectra of Si LVV and Si KLL of the PEE samples PEE5, PEE6 and PEE7. The curves for Si, thermal SiO_2, CVD-Si_3N_4 and PEO (plasma enhanced oxidation) oxide are shown for reference. With growing concentration of incorporated oxygen in the PEE-SiON samples the Si KLL peak shifts as expected from 76 to 84 eV, the literature values for SiO_2 and Si_3N_4 [17]. All stoichiometric and substoichiometric oxides grown by any method were found to be uniform by AES in depth distribution.

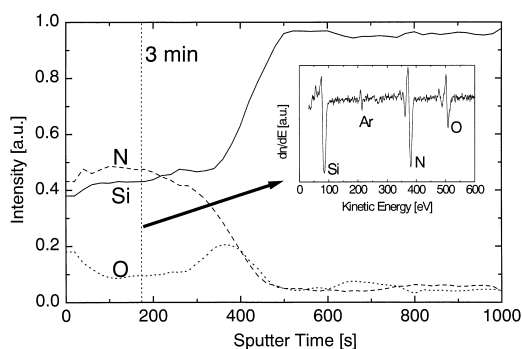

Fig. 6. AES depth profile of SiON sample PEE5. The surface spectrum after a part of the bulk layer was removed verifies the atomic concentrations.

It was further found by AES that more O than N species were incorporated into the thin PEO films grown in pure N_2 plasma. No nitrogen was detectable in the film grown in an N_2/O_2 plasma with 5 sccm of each gas. The bulk mainly consists of SiO_2.

4.2. X-ray photoelectron spectroscopy (XPS)

The XPS survey spectra of all substoichiometric oxides before sputtering show a small amount of adventitious C and native oxide, of which both were removed by sputtering. This is demonstrated in Fig. 8 with the sample GEE5. After sputtering, the Si 2p as well as the O 1s peaks are slightly broadened, even for the thermal SiO_2 and the CVD-

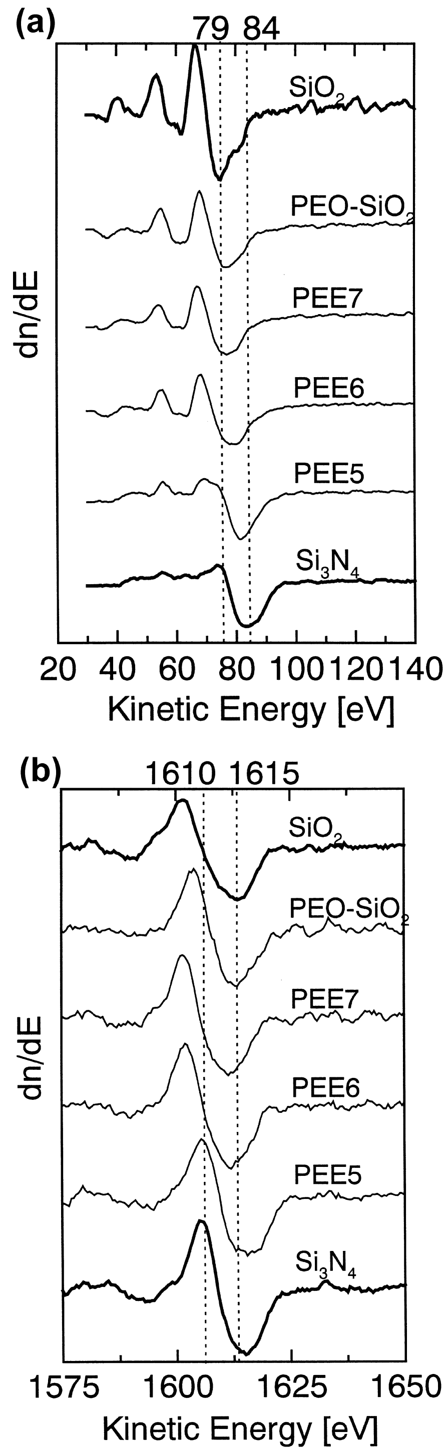

Fig. 7. Changes of the (a) Si LVV and (b) Si KLL Auger spectra of PEE SiON films as a function of refractive index. The curves of PEO-SiO_2, thermal SiO_2 and of elemental Si are shown for comparison. The dashed lines give the literature values of the bottom peak of Si LVV (76 eV for SiO_2, 84 eV for Si_3N_4) and Si KLL (approximately 1610 eV for SiO_2, 1615 eV for Si_3N_4) [17]. The O_2:N_2 gas mixture was 4:4, 2:6 and 0:8 sccm for the samples PEE7, PEE6, and PEE5, respectively.

Si_3N_4 specimen. This can be attributed to slight lattice damage caused by ion bombardment. Fig. 9 shows the high resolution Si 2p spectra of GEE grown oxides

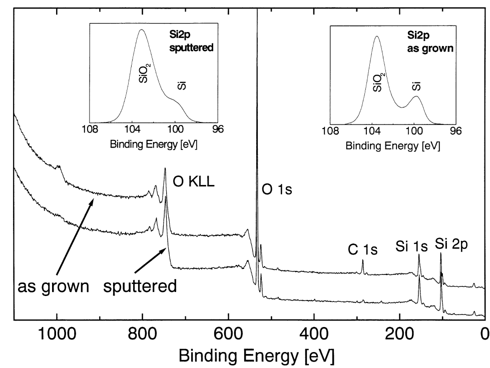

Fig. 8. Survey spectrum of SiO_x sample GEE5 before and after sputter-cleaning.

compared with those of thermal SiO_2 and the Si substrate with the peak positions close to the literature values of 103.3 and 99.3 eV, respectively [21]. As already demonstrated by the AES spectra, the peak of the SiO_x films is broadened or even split depending on the composition. This indicates the presence of more than one oxidation state.

The quantity of Si in the films was determined from the XPS spectra as follows. The background was subtracted from the Si 2p peak. Five symmetric Gaussian bands representing the different valence states Si, Si^{+}, Si^{2+}, Si^{3+} and Si^{4+} were added with the maximum at binding energies of 99.4, 100.3, 101.3, 102.2, and 103.4 eV with a tolerance of $\pm$ 0.2 eV. The FWHM was fixed to 1.4 $\pm$ 0.2 eV for all states except for the Si^{4+} subband where 1.7 $\pm$ 0.2 eV was used. The peak positions and the FWHM values are in good agreement with those in the literature [22,23]. Elemental Si and Si–H differ by only 0.35 eV and were thus fitted as a single peak [24]. The average atomic concentration ratio $x = \mathrm{O} : \mathrm{Si}$ was calculated by the Si 2p subbands as follows [23]

$$x = \frac{1}{2}\left(\sum_{n=1}^{4} nA(\mathrm{Si}^{n+})/\sum_{n=0}^{4} A(\mathrm{Si}^{n+})\right) \quad (1)$$

Here, $A(\mathrm{Si}^{n+})$ represents the relative amount of the Si valence states from the curve fits, which were determined

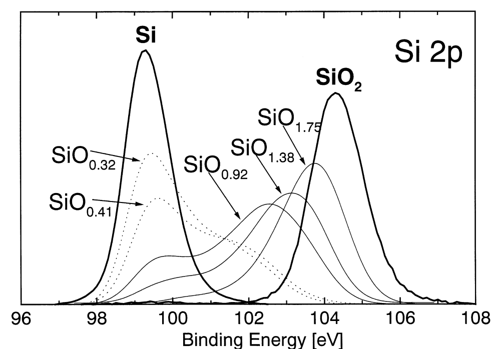

Fig. 9. Si 2p spectra measured by XPS of silicon suboxides grown by GEE (straight line) and PEE (dashed line). The curves of thermal SiO_2 and of elemental Si are shown for comparison.

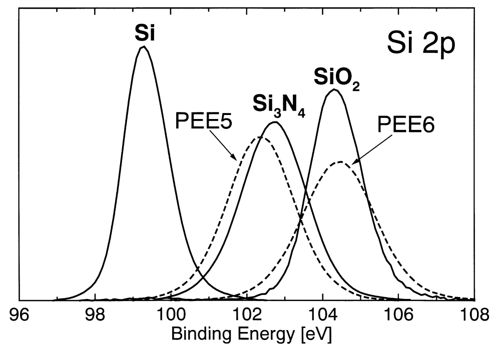

Fig. 10. Si 2p spectra measured by XPS of silicon oxynitrides grown by PEE. The curves of thermal SiO_2, CVD-Si_3N_4 and of elemental Si are shown for comparison.

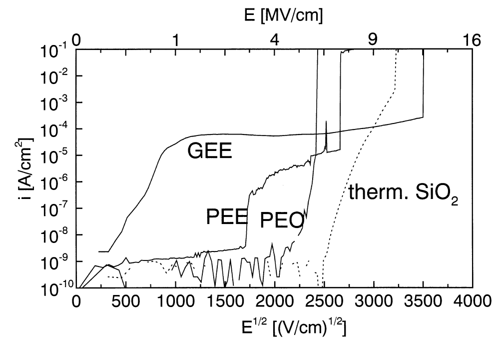

Fig. 12. Comparison of *I–V* characteristics of different low-temperature oxides in MOS structures. The curve of thermal SiO_2 is shown for reference.

by calculating the area under each subpeaks. For the silicon oxynitride samples this method is difficult because there are too many valence states possible. Thus the conventional method of comparing different peak areas normalized by relative sensitivity factors given in [21] was used to roughly estimate the element concentrations.

Fig. 10 shows the Si 2p spectra of some oxynitrides. The peak position of PEE5 nearly equals that of CVD-Si_3N_4. The slight shift to smaller binding energies is attributed to a surplus of Si. The Si 2p spectrum of PEE6 is not shifted from that of thermal SiO_2 because the film only contains about 3% nitrogen. The large FWHM indicates the presence of other phases than SiO_2 in the film.

RBS spectra were taken from some GEE samples. The elemental concentrations determined by this method compare well with the XPS results as can be seen in Table 2. The thickness obtained by RBS is about 10–20% higher than the ellipsometer values. Thus, the deposited films are less dense than thermal oxides. This fits well with the earlier discussion of the AES results.

Regarding film composition, the AES and XPS results lead to the conclusion that silicon oxides of different stoichiometries can be fabricated by GEE depending on process parameters. For the plasma-assisted processes PEE and PEO, oxynitrides can be formed in addition. Since no evaporated silicon is offered during substrate oxidation, only SiO_2 and no sub-oxides were formed by PEO.

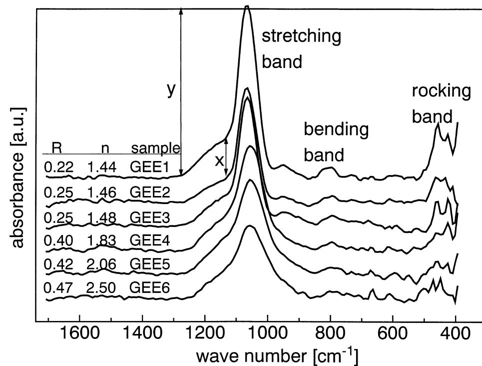

Fig. 11. Infrared absorption spectra of as-deposited SiO_x films grown by GEE.

4.3. Infrared spectroscopy (IR)

The IR spectra in the region of 400–1600 cm^{-1} in Fig. 11 show the Si–O stretching, bending and rocking band of GEE-grown SiO_x. The shoulder height of the main Si–O stretching bend divided by the peak height y is defined as the ratio R, thus $R = x/y$ [25]. R is a function of film composition ranging from 0.22 for SiO_2 to 0.47 for Si rich $SiO_{0.92}$ ($n = 2.50$). Compared with the XPS results, samples with n close to 1.46 have their stretching peak all at 1066 cm^{-1}. For samples with n greater than 1.48 (see Table 2) the Si–O stretching frequency shifts towards lower wave numbers below 1057 cm^{-1}. The spectra of the stoichiometric samples exhibit an extra absorption band in the region of 900–980 cm^{-1} between the bending and the stretching band. This extra peak merges with the broadened stretching band of the Si rich samples and is probably associated with the Si–H bending mode in H_2SiO_2 groups [26]. The GEE films are too thin to clearly detect any Si–H or Si–OH absorption bands. Due to the limits of this method, it can only be concluded that the films contain Si–O compounds. The changes of the shoulder heights agree with the results on stoichiometry obtained from XPS.

4.4. Electrical characterization

The relation between the leakage current and the electric field of one typical representative of the PEE-, GEE- and PEO-grown stoichiometric oxides is plotted in Fig. 12. The curve of a wet thermally grown oxide is shown for reference. The PEO sample exhibits no current injection until 4 MV/cm. The displacement current due to the voltage ramp is below 1×10^{-9} A/cm^2. Some Fowler–Nordheim tunneling seems to occur before breakdown below 6 MV/cm. There is no current injection due to charge trapping. A different behaviour is shown by the PEE sample. Below 3 MV/cm a tiny displacement current of the order of 10^{-9} A/cm^2 is present. Above 3 MV/cm electrons are injected, filling deep traps in the bulk of the oxide. This results in a ledge

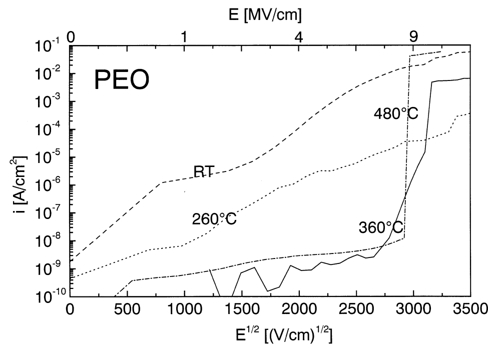

Fig. 13. Comparison of *I–V* characteristics of PEO oxides in MOS structures grown at different substrate temperatures.

of the logarithmic *I–V* plot for the trapped charge carriers oppose the applied external field [27]. This plateau further presents some noise and a current spike as a result of a localized breakdown. After all traps are filled, destructive breakdown occurs at nearly 7 MV/cm for this specimen. The *I–V* characteristics of the GEE-grown sample is rather poor.

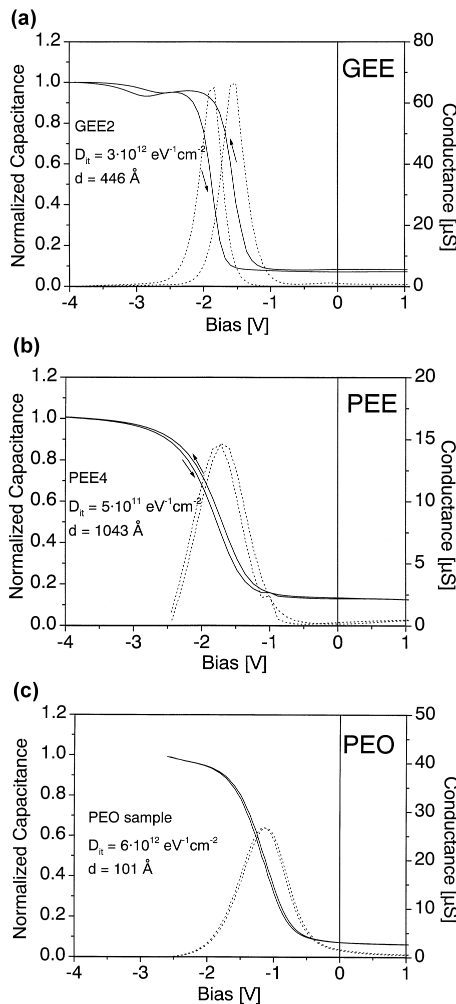

Fig. 14. Trace and retrace *C–V* characteristics of SiO_2 grown by (a) GEE, (b) PEE, (c) PEO

High current injection occurs at even very low fields under 2 MV/cm. The current saturates between 10^{-5} and 10^{-4} A/ cm^2 until the high breakdown field of 13 MV/cm. There are two effects responsible for the shift of the destructive breakdown to this very high field. First, the high conductance of the oxide reduces the applied external field in the MOS capacitor. Second, the presence of a large number of charge traps and the build-up of new traps provide a high opposing internal field retarding the breakdown. New traps in the dielectric layer during the voltage ramp can originate due to local heating, caused of the high current flow [27].

According to our observations, the electrical characteristics of GEE and PEE oxides hardly depend on the substrate temperature during growth. The *I–V* curves of PEO samples improve with increasing substrate temperature, however. Fig. 13 shows that significant current injection occurs in films fabricated at room temperature and at 260°C. In the films produced at 360 and 480°C there is no significant leakage current until the breakdown field is reached.

The excellent dielectric strength makes the PEO oxide a very promising candidate for applications like passivation of vertical MBE-grown devices (this was already shown in [28]) or as a high-field dielectric between the control gate and the floating gate in EPROM devices [3]. Furthermore, the *I–V* characteristics from wafer to wafer are highly reproducible. A PEE oxide of the above-shown *I–V* curve can be used as a somewhat thicker passivation layer for nano- and microelectronic devices and as an intermetal dielectric below metallic surfaces. The *I–V* curves are fairly reproducible and can be improved by optimizing the process parameters. The poor bulk resistivity of the GEE sample is not acceptable for most electronic devices where very thin dielectrics are needed. The high current injection and the trapping ledge are fairly reproducible from wafer to wafer. Sometimes the destructive breakdown occurs at very low fields.

Fig. 14a–c compares the trace and retrace high-frequency *C–V* and *G–V* curves of the low-temperature oxides. The negative flatband voltage of all dielectrics indicates that positive charge exists either at the interface or within the bulk layer. The hysteresis between the trace and retrace curve of the GEE and PEE sample is caused by the interchange of charge carriers across the silicon-insulator interface. Holes could be emitted from traps in the insulator and trapped in the oxide, or electrons could be emitted from traps in the insulator and transported into Si. Both effects contribute to hysteresis [29]. This observation is consistent with the *I–V* characteristics where carrier injection even occurs at rather low fields. The very low hysteresis of 0.2 V and the flatband voltage of only $-$ 1.2 V indicate low densities of mobile and fixed charges within the PEO oxide layer. This is in accordance with the *I–V* curve where no trapping ledge occurs before breakdown.

The interface state density D_{it} lies between the medium 10^{11} to low 10^{12} eV^{-1} cm^{-2} range for the low-temperature samples. There occurs no change between the measure-

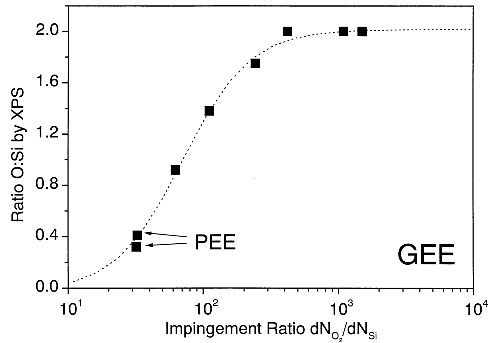

Fig. 15. O:Si ratio in GEE films as a function of the impingement ratio of evaporated silicon and oxygen gas.

ments of the trace and retrace measurement. This is rather poor for applications as gate oxides. Obviously the different growth kinetics for such low temperatures are responsible for the high interface state density. The D_{it} values of unannealed thermal SiO_2 and CVD-Si_3N_4 are 1.2×10^{11} and 2.0×10^{11} eV^{-1} cm^{-2}, respectively. No postmetallization anneal was performed.

5. Discussion of film growth

5.1. Gas enhanced evaporation (GEE)

The deposition of SiO_x is performed by reactive evaporation of Si in O_2 atmosphere. O_2 naturally reacts with the Si surface. The composition of the deposited film is supposed to depend on three parameters: the evaporation rate of Si, the oxygen pressure and the wafer temperature. At O_2 pressures higher than approximately 2×10^{-2} Pa the mean free path of the evaporated Si is lower than the distance between the Si target and the Si substrate. Consequently, at pressures lower than 2×10^{-2} Pa the probability of the formation of molecules like SiO or even SiO_2 through collisions in the gas phase is very small. The chemical reactions take place on the surface of the substrate and later on the growing film, which is exposed to the impingement of Si atoms and molecules as well as to O_2 molecules. The particles are adsorbed, reflected, or desorbed after a short contact with the surface. The reaction of the adsorbed species is supported by surface diffusion into the potential wells of the regular lattice sites [30]. Hence, the kinetics of the film growth is controlled by the impingement rates of the participating species, their condensation coefficients and the substrate temperature. The condensation coefficient is the ratio of permanently adsorbed to total impinging particles on the surface. The impingement rates of the evaporant as well as of the reactive gas can be calculated or graphically determined by a nomogram [30] if the gas pressure and the deposition rate with the absence of any gas are known. Fig. 15 describes the dependence of the film composition, i.e. the stoichiometry as determined by XPS, on the impingement ratio of Si and O_2. It can be clearly seen that SiO_2 is obtained if the oxygen pressure is increased beyond a certain value.

A further increase of the impingement ratio can negatively affect the film properties. We observed a decrease of the refractive index down to 1.42 for GEE-grown samples at oxygen pressures far greater than 2×10^{-2} Pa (Fig. 4). A refractive index lower than the theoretical value of 1.465 (for thermal SiO_2) is attributed to porousity or low density of the film [31]. Possible reasons are the increased number of collisions and the associated energy loss of the evaporated Si particles at high gas pressures. Now, molecules like SiO or SiO_2 are likely to hit the surface. The growth of a high quality film (i.e. a film with high density in this case) is impeded by the reduced surface diffusion of rather large species like SiO. Film quality (like electrical performance or film density) could be improved by substrate temperatures higher than 450°C leading to enhanced surface diffusion.

The high density of interface states of all oxide samples can also be explained by the film growth kinetics. At low growth temperatures surface migration of adsorbates is suppressed. The Si surface dangling bonds cannot be passivated effectively through chemical bonding. Si dangling bonds usually act as a source of positive fixed charges in the oxide [32]. This can cause problems such as trapping and detrapping of electrons if an electrical field is applied. The electron injection rate is enhanced at high interface state densities because electrons can easily enter the oxide by tunneling when dangling bonds exist at the interface. It was observed by mass spectroscopy that evaporated Si mainly consists of atomic Si but also of clusters like Si_2 or Si_3. Thereby, unoxidized Si islands are formed in the film which can act as a trap for positive fixed charges when interfacially polarized [33]. For GEE as deposition process, the original Si surface corresponds to the SiO_2/Si interface. Hence, the interface properties depend strongly on the Si surface condition before growth. Special care must be taken with substrate cleaning.

5.2. Plasma enhanced oxidation (PEO) and plasma enhanced evaporation (PEE)

For PEO and PEE, two additional plasma-generated reactive species, atomic and negatively charged oxygen (O^-) [20], as well as an additional gas, Ar, are present, of which the latter is necessary to maintain the discharge. To keep the plasma stable, a minimum of 20 sccm Ar flow, corresponding to 6×10^{-2} Pa, is necessary. At this pressure the mean free path of the evaporated Si is below but still of the same order of the distance crucible - substrate. Thus, high evaporation rates are necessary to compensate the loss of evaporated Si by scattering with Ar and O_2.

With an arc current of $I_{arc} = 25$ A, the arc voltage typically amounts to $U_{arc} = 45$ V. The number N of the electrons in the arc is obtained from the relation

$$I_{arc} \cdot t = N \cdot e \qquad (2)$$

where e is the electron charge and t the time. The electrons are emitted from the filament and accelerated over a distance of 50 cm from the filament to the opposite chamber wall. This yields for the number of electrons

$$N = \frac{I_{arc} \cdot s}{e}\sqrt{\frac{2m}{e \cdot U_{arc}}} \tag{3}$$

where the electron mass and the distance are represented by m and s, respectively. With the arc radius r estimated to 5 cm the electron density in the arc is calculated as follows

$$n = \frac{N}{s \cdot r^2 \cdot \pi} = 1.0 \times 10^{10} \left(\mathrm{cm}^{-3}\right) \tag{4}$$

The density of the present O_2 molecules in the chamber is obtained from the ideal gas equation to

$$n(O_2) = \frac{p(O_2)}{k \cdot T} = 4.8 \times 10^{12} \left(\mathrm{cm}^{-3}\right) \tag{5}$$

Here, p is the O_2 partial pressure (2×10^{-2} Pa) and T is the temperature, which is supposed to be 300 K.

The growth kinetics of PEO is similar to thermal oxidation and has been previously discussed in brief in this paper. At the beginning of film growth, oxidizing ionic species are transported rapidly by the bias difference between the plasma and the wafer to the interface [20]. The film growth is thus reaction limited. When the layer becomes thicker, the diffusion time reduces the growth speed which is now parabolic (slope (1/2) in Fig. 2). The afore-mentioned difference in bias as well as the small size of atomic O and ionic O^- as compared to molecular O_2 are the driving forces for the rapid oxide growth as compared to thermal oxidation. The growth rate of PEO oxides is typically 0.05 Å/s at 450°C for long process times.

The number of atomic oxygen, which is necessary for SiO_2 film growth is determined as follows. The oxidation rate Φ per area of the interface Si atoms is given by

$$\Phi(\mathrm{Si}) = \frac{dN_{\mathrm{Si}}}{dt \cdot dA} = \frac{\rho_{\mathrm{Si}} \cdot N_A}{M_{\mathrm{Si}}} R \tag{6}$$

Here, N_{si} is the number of oxidized Si atoms at the substate's surface, t is the time of plasma exposure, A is the oxidized area, N_A Avogadro's constant, M_{Si} is the molecular mass of Si (28.09 g/mol), ρ_{Si} the density of crystalline Si (2.32 g/cm^3), and R is the SiO_2 film growth rate, given by film thickness per oxidation time t.

With the film growth rate of 0.05 Å/s and taking into account that two oxygen atoms react with one silicon atom of the crystal the following flux of oxygen atoms per time and area towards the Si substrate is necessary

$$\Phi(O) = \frac{dN_{\mathrm{Si}}}{dt \cdot dA} = 2 \cdot \Phi(\mathrm{Si}) = 5 \times 10^{13} \left(\mathrm{s}^{-1}\mathrm{cm}^{-2}\right) \tag{7}$$

With the approximation that the plasma particles exhibit the Maxwell velocity distribution [34] the square root of the mean squared velocity v is given by

$$\sqrt{\overline{v^2}} = \sqrt{\frac{3 \cdot k \cdot T}{m_O}} = 6.8 \times 10^4 \ (\mathrm{cm}/s) \tag{8}$$

where m_O is the mass of atomic oxygen. For an isotropic velocity distribution only one sixth of the atoms and ions reach the Si surface and that all of these atoms migrate through the growing film to the substrate, the following density of non-molecular O species, which can contribute to oxidation is calculated to

$$n(O) = \frac{6 \cdot \Phi(O)}{\sqrt{\overline{v^2}}} = 4.4 \times 10^9 \left(\mathrm{cm}^{-3}\right) \tag{9}$$

If this value is compared with the electron density in the arc one can conclude that with our experimental conditions one or two electrons create one pair of atomic O, of which most of them reach the Si substrate by diffusion through the growing film at 450°C substrate temperature. Compared with the density of O_2 molecules in the chamber, only one over 1000 molecules is dissociated.

Especially, the PEO process buries the SiO_2/Si interface below the original surface. The interface properties are thus independent of the subsequent oxide formation, but rather depend on the low-rate plasma oxidation process. Thereby, better electrical properties are obtained than by GEE. This can be clearly seen by the low charge carrier injection of the PEO oxides compared to GEE oxides if an external electrical field is applied (Fig. 12).

PEE combines both oxidation methods, GEE and PEO. The film grows by oxidation of the adsorbed Si on the surface as well as by diffusion of atomic O into the film. At the beginning of film growth, the interface is buried below the original substrate surface by diffusion of atomic O, known as subcutaneous oxidation. When the film becomes thicker, it is more likely that dangling bonds of Si rich nano-clusters in the deposited layer serve as a sink for O radicals. Then, fewer O species reach the interface. In a word, subcutaneous oxidation is reduced with increasing film growth and with increasing Si content in the deposited film.

It was shown that GEE works well in O_2 but not in N_2 atmosphere. The reactive Si dangling bonds do not adsorb N_2 for its high inertness. Hence, N_2 must be dissociated before in the electron arc. However, the PEO oxynitride films grown in an Ar/N_2 plasma without oxygen mainly consist of SiO_2 instead of Si_3N_4 and are rather thin compared to PEO oxides grown under the same conditions. This is expected because Si_3N_4 and oxynitrides serve as a diffusion layer for atomic species [35]. During the plasma process, oxygen desorbs from the chamber walls by electron and ion bombardment and is thus always present in the plasma. In addition, the dissociation energy of the inert gas N_2 (9.8 eV) is much higher than for O_2 (5.2 eV) [36]. This explains why the formation of silicon oxide is much more likely than the formation of silicon nitride even if only N_2 is added to the plasma. The sample PEE5 mainly contains silicon nitride

but is rather silicon rich. The reason is that only very few electrons in the low-energy plasma have enough energy to crack the N_2 molecule. Furthermore, if the nitride samples are carried through air to the measurement apparatus, the surface is heavily oxidized by the surrounding air.

6. Conclusions

Low-temperature oxides and suboxides were fabricated by the following plasma and evaporation-assisted processes on Si substrates: gas enhanced evaporation, plasma enhanced oxidation and by a combination of both processes, called plasma enhanced evaporation. The extensive characterization of the films show that stoichiometry is controlled by the impingement ratio of the oxygen and silicon species on the substrate surface for GEE and PEE. PEO is comparable to thermal oxidation because both are diffusion processes. The difference is that O radicals produced by the plasma migrate much faster through the film than O_2 molecules. According to XPS and AES measurements all oxidation states of silicon can be present in the same film depending on the Si:O concentration ratio in the film. The electrical properties are rather determined by the different growth kinetics than by a change of process parameters. The very good *I–V* characteristics are mainly due to the buried SiO_2/Si interface. The electrical quality of SiO_2 deposited by GEE is rather poor because of low film density and possibly because of incorporated Si rich clusters not detectable by AES or XPS. Due to subcutaneous plasma oxidation, PEE oxides show better electrical properties than GEE films. The low substrate temperature during film growth opens up numerous applications for these processes.

Acknowledgements

The authors like to thank J. Messarosch, G. Fehlauer, H. Baumgärtner, F. Kaesen, H. Geiger, V.R. Rao and T. Pompl for their assistance in electrical measurements, sample preparation and fruitful discussions. The expertise of J. Ramm, E. Beck and R. Slepicka of Balzers AG is greatfully acknowledged. This work was supported by the BMBF under grant no. BA-672. One of the authors, A. Strass, likes to thank the German Academic Exchange Service (DAAD) for financial assistance during his scientific stay at the Universidad de Chile.

References

[1] M. Nakamura, Y. Mochizuki, K. Usami, Y. Itoh, T. Nozaki, J. Electrochem. Soc. 132 (1985) 482.
[2] K. Machida, N. Shimoyama, J. Takahashi, N. Yabumoto, E. Arai, IEEE Trans, Electron. Devices 41 (1994) 709.
[3] J. Makwana, B. Grula, D. Monteilh, R. Tyldesley, A. Sorensen, Semiconduct. Int. 10 (1997) 125.
[4] J.H. Magerlein, J.M. Baker, G.R. Proto, K.R. Grebe, S.P. Klepner, M.J. Palmer, A.J. Warnecke, J. Vac. Sci. Technol. B 2 (4) (1984) 636.
[5] N. Chand, et al., J. Cryst. Growth 148 (1995) 336.
[6] D.C. Diaz, C.L. Schow, J. Qi, J.C. Campbell, J.C. Bean, L.J. Peticolas, Appl. Phys. Lett. 69 (19) (1996) 2798.
[7] A. Durandet, A. Perry, R.W. Boswell, et al., Electron. Lett. 32 (4) (1996) 326.
[8] S.K. Ghandhi, VLSI Fabrication Principles, 2nd ed., Wiley, New York, 1993 Chapter 8.
[9] S. Fujita, M. Nishihara, W.L. Hoi, A. Sasaki, Jpn. J. Appl. Phys. 20 (1981) 917.
[10] B.J. Standbery, et al., Solut. Cells 14 (1985) 289.
[11] The National Technology Roadmap for Semiconductors, SIA Semiconductor Industry Association, 1994, p. 103.
[12] H. Gossner, I. Eisele, L. Risch, Jpn. J. Appl. Phys. 33 (1) (1994) 2423.
[13] B. Fowler, E. O'Brien, J. Vac. Sci. Technol. B 12 (1) (1994) 441.
[14] A. Strass, W. Hansch, P. Bieringer, A. Neubecker, F. Kaesen, A. Fischer, I. Eisele, Surf. Coat. Technol. 97 (1997) 158.
[15] W. Hansch, E. Hammerl, W. Kiunke, I. Eisele, J. Ramm, E. Beck, Jpn. J. Appl. Phys. 33 (1) (1994) 2263.
[16] J. Ramm, E. Beck, A. Dommann, I. Eisele, D. Krüger, Thin Solid Films 246 (1994) 158.
[17] L.E. Davis, N.C. MacDonald, P.W. Palmberg, G.E. Riach, R.E. Weber, Handbook of Auger Electron Spectroscopy, Physical Electronics Industries, Eden Prairie, 1976.
[18] B.E. Deal, A.S. Grove, J. Appl. Phys. 36 (1965) 3770.
[19] I. Brodie, J.J. Muray, The physics of Microfabrication, Plenum, New York, 1982.
[20] Y.Z. Hu, Y.Q. Wang, M. Li, E.A. Irene, J. Vac. Sci. Technol. A 4 (11) (1993) 900.
[21] J.F. Moulder, W.F. Stickle, P.E. Sobol, K.D. Bomben, Handbook of XPS, Physical Electronics Industries, Eden Prairie, 1992.
[22] R. Alfonsetti, L. Lozzi, M. Passacantando, P. Picozzi, S. Santucci, Appl. Surf. Sci. 70/71 (1993) 222.
[23] J.R. Shallenberger, J. Vac. Sci. Technol. A 14 (3) (1996) 693.
[24] H. Niwano, Y. Katakura, Y. Takeda, N. Takakuwa, M. Myamoto, J. Vac. Sci. Technol. A 9 (1991) 195.
[25] P.G. Pai, S.S. Chao, Y. Takagi, G. Lucovsky, J. Vac. Sci. Technol. A 4 (1986) 689.
[26] D.V. Tsu, G. Lucovsky, B.N. Davidson, Physical Rev. B 40 (1989) 1795.
[27] D.J. DiMaria, R. Ghez, D.W. Wong, J. Appl. Phys. 51 (9) (1980) 4830.
[28] A. Strass, W. Hansch, F. Kaesen, G. Fehlauer, P. Bieringer, A. Fischer, I. Eisele, 7th Int. Symp. Si MBE, Thin Solid Films, 321 (1998) 261--264.
[29] T.L. Chu, J.R. Szedon, C.H. Lee, Solid State Electron. 10 (1967) 897.
[30] L.I. Maissel, R. Glang, Handbook of Thin Film Technology, McGraw-Hill, New York, 1970.
[31] T.V. Herak, T.T. Chau, D.J. Thomson, S.R. Mejia, D.A. Buchanan, J. Kao, Phys. 65 (6) (1994) 2457.
[32] Y.-B Park, J.-K. Kang, S.-W. Rhee, Thin Solid Films 280 (1996) 43.
[33] P. Dimitrakis, G.J. Papaioannou, J. Appl. Phys. 80 (3) (1996) 1605.
[34] M. Konuma, Film deposition by plasma techniques, Springer–Verlag, Berlin, 1992.
[35] B.E. Deal, E.L. McKenna, P.L. Castro, J. Electrochem. Soc.: Solid State Sci. 116 (7) (1969) 997.
[36] Chemical Rubber Company, CRC Handbook of Chemistry and Physics, 73rd ed., 1993.